How to cite: *Angew. Chem. Int. Ed.* **2021**, *60*, 24694–24701
International Edition: doi.org/10.1002/anie.202111163
German Edition: doi.org/10.1002/ange.202111163

Enzyme Catalysis

Unexpected Reactions of α,β-Unsaturated Fatty Acids Provide Insight into the Mechanisms of CYP152 Peroxygenases

Yuanyuan Jiang[+], Wei Peng[+], Zhong Li[+], Cai You, Yue Zhao, Dandan Tang, Binju Wang, and Shengying Li**

Abstract: *CYP152 peroxygenases catalyze decarboxylation and hydroxylation of fatty acids using H_2O_2 as cofactor. To understand the molecular basis for the chemo- and regioselectivity of these unique P450 enzymes, we analyze the activities of three CYP152 peroxygenases ($OleT_{JE}$, $P450_{SP\alpha}$, $P450_{BS\beta}$) towards cis- and trans-dodecenoic acids as substrate probes. The unexpected 6S-hydroxylation of the trans-isomer and 4R-hydroxylation of the cis-isomer by $OleT_{JE}$, and molecular docking results suggest that the unprecedented selectivity is due to $OleT_{JE}$'s preference of C2–C3 cis-configuration. In addition to the common epoxide products, undecanal is the unexpected major product of $P450_{SP\alpha}$ and $P450_{BS\beta}$ regardless of the cis/trans-configuration of substrates. The combined $H_2{}^{18}O_2$ tracing experiments, MD simulations, and QM/MM calculations unravel an unusual mechanism for Compound I-mediated aldehyde formation in which the active site water derived from H_2O_2 activation is involved in the generation of a four-membered ring lactone intermediate. These findings provide new insights into the unusual mechanisms of CYP152 peroxygenases.*

Introduction

Cytochrome P450 enzymes (CYPs or P450s) catalyze diverse oxidative reactions towards a myriad of natural and unnatural substrates, thus being named the most versatile biocatalysts in nature.[1] A vast majority of P450s share a common monooxygenation mechanism that requires O_2, NAD(P)H, and redox partner(s) as the oxygen donor, electron source, and electron shuttle(s), respectively. However, a handful of P450s such as CYP152 peroxygenases have evolved the ability to directly utilize H_2O_2 as the sole oxygen and electron donor to drive the P450 catalysis via a so-called peroxide shunt pathway.[2]

The P450 peroxygenase $OleT_{JE}$ (CYP152L1) from *Jeotgalicoccus* sp. ATCC 8456 has been attracting great attention from the fields of both biofuels and biomaterials in the past decade because it catalyzes a single-step oxidative decarboxylation of fatty acids (C_n: $n = 4$–20) to form α-olefins (C_{n-1}) as value-added products using H_2O_2 as cofactor (Figure 1a).[3] By contrast, the fatty acid α-hydroxylase $P450_{SP\alpha}$ (CYP152B1) from *Sphingomonas paucimobilis* and the fatty acid β-hydroxylase $P450_{BS\beta}$ (CYP152A1) from *Bacillus subtilis* preferentially convert fatty acids into α- and β-hydroxy fatty acids, respectively.[4] Mechanistically, it has been widely accepted that the three most-studied CYP152 enzymes activate H_2O_2 via the substrate-assisted heterolytic cleavage of the peroxy bond to generate the iron(IV) oxo π cation radical (Compound I, *abbr.* Cpd I) species, which is responsible for abstracting the C_α- or C_β-hydrogen from the fatty acid substrates. Differentially, $P450_{SP\alpha}$ exclusively abstracts C_α–H to generate the substrate radical at C_α position, thereby yielding α-hydroxy fatty acid via a normal OH rebound mechanism; whereas $P450_{BS\beta}$ and $OleT_{JE}$ prefer C_β–H abstraction and the different fates of the C_β radical give rise to α-olefin ($OleT_{JE}$) and β-hydroxy fatty acid ($P450_{BS\beta}$) as the major products (Figure S1).[2a,3b,4c,d,5] Of note, both $P450_{BS\beta}$ and $OleT_{JE}$ can produce a small amount of α-hydroxy fatty acid as side product, indicative of their lower regioselectivity than $P450_{SP\alpha}$.

[*] Dr. Y. Jiang,[+] Dr. Z. Li,[+] Dr. C. You, Dr. D. Tang, Prof. Dr. S. Li
State Key Laboratory of Microbial Technology
Shandong University
No. 72 Binhai Road, Qingdao, Shandong 266237 (China)
E-mail: lishengying@sdu.edu.cn

Dr. Y. Jiang,[+] Dr. Z. Li[+]
Shandong Provincial Key Laboratory of Synthetic Biology
CAS Key Laboratory of Biofuels
Qingdao Institute of Bioenergy and Bioprocess Technology
Chinese Academy of Sciences
No. 189 Songling Road, Qingdao, Shandong 266101 (China)

Dr. Y. Jiang,[+] Dr. Z. Li,[+]
University of Chinese Academy of Sciences
Beijing 100049 (China)

W. Peng[+] Prof. Dr. B. Wang
State Key Laboratory of Physical Chemistry of Solid Surfaces and Fujian Provincial Key Laboratory of Theoretical and Computational Chemistry
College of Chemistry and Chemical Engineering
Xiamen University
Xiamen 361005 (China)
E-mail: wangbinju2018@xmu.edu.cn

Y. Zhao
Key Laboratory of Combinatorial Biosynthesis and Drug Discovery
Ministry of Education
School of Pharmaceutical Sciences, Wuhan University
Wuhan 430071 (China)

Prof. Dr. S. Li
Laboratory for Marine Biology and Biotechnology
Qingdao National Laboratory for Marine Science and Technology
Qingdao, Shandong 266237 (China)

[+] These authors contributed equally to this work.

Supporting information and the ORCID identification number(s) for the author(s) of this article can be found under: https://doi.org/10.1002/anie.202111163.

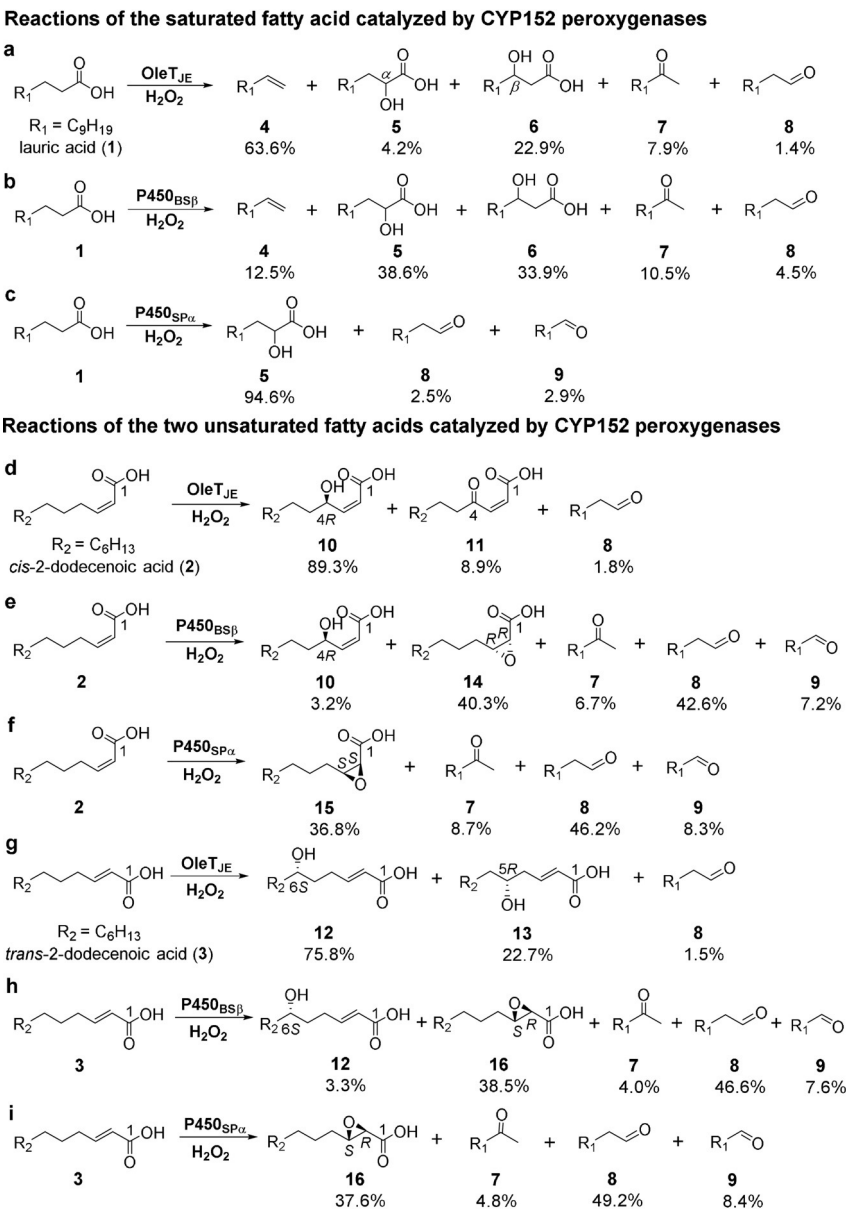

Figure 1. Reactions catalyzed by CYP152 peroxygenases towards three different C_{12} fatty acids **1**–**3**. The percentage ratios are shown for each individual product. Reaction conditions: 1 μM P450, 500 μM substrate (**1**, **2**, or **3**), 5 μM AldO, and 10% glycerol at 30°C for 6 h. Unless otherwise specified, the product distribution of the reaction system using exogenously added H_2O_2 as cofactor is similar to that of the corresponding AldO/glycerol system for in situ gradual H_2O_2 generation.

To understand the underlying mechanisms for the distinct chemo- and regioselectivity of three representative CYP152 family members that share significant similarity in protein sequences (Figure S2), a growing number of mechanistic studies have been conducted. For example, structural analysis and product profiling of abundant mutants indicated that accurate positioning of substrate is essential for the selectivity of $OleT_{JE}$.[3b,6] Substrate kinetic isotope effect and QM/MM studies confirmed that the decarboxylation results from substrate C_β–H abstraction by Cpd I.[5a,b] Furthermore, computational studies revealed that the reactivity of $OleT_{JE}$ is mostly determined by the regioselective H-abstraction from the substrate by Cpd I; that is, a weaker C_β–H bond initiates either β-hydroxylation or decarboxylation while a weaker C_α–H bond leads to α-hydroxylation and the desaturation of α-methylated fatty acids.[7]

Despite this significant progress, it remains unclear how the conformational and electronic properties of substrates would affect the catalytic outcome of CYP152 peroxygenases because all previous mechanistic studies unanimously utilized the saturated fatty acids as testing substrates. To address these issues, herein, *cis*- and *trans*-2-dodecenoic acid (α,β-unsaturated C_{12} fatty acids) were selected as substrate probes for comparative catalytic analysis (chemoselectivity, product profile, and catalytic efficiency) of $OleT_{JE}$, $P450_{BS\beta}$, and $P450_{SP\alpha}$ with complementary experimental and computational approaches.

Results and Discussion

Identification of distinct regioselective hydroxylation activities of P450 fatty acid decarboxylase $OleT_{JE}$. The oxidative transformations of lauric acid (**1**; the $OleT_{JE}$-preferred substrate was used as a reference), *cis*-2-dodecenoic acid (**2**), and *trans*-2-dodecenoic acid (**3**) by $OleT_{JE}$ were first investigated using either the exogenous H_2O_2 addition system or the AldO/glycerol-based in situ H_2O_2 releasing system.[8] As a control reaction (1 μM P450, 500 μM substrate, 5 μM AldO, and 10% glycerol at 30°C for 6 h), $OleT_{JE}$ converted 100% (88.1% for the exogenous H_2O_2 addition system) of **1** into a mixture of three known products including 1-undecene (**4**; relative product ratio = 63.6%), α-hydroxy-lauric acid (**5**; 4.2%), and β-hydroxy-lauric acid (**6**; 22.9%), and two newly identified minor products 2-undecanone (**7**; 7.9%, presumably due to over-oxidation of **6**) and undecanal (**8**; 1.4%, see below for the putative mechanism; Figure 1a).

Towards the *cis*-α,β-unsaturated fatty acid substrate, with a 100% substrate conversion, $OleT_{JE}$ mainly catalyzed the γ-hydroxylation of **2**, giving rise to 4*R*-hydroxy-*cis*-2-dodecenoic acid (**10**; 89.3%, Figure 1d), whose structure was determined by mass spectrometry (MS) and nuclear magnetic resonance (NMR) analyses (Table S2, Figures S3–S16). Further electronic circular dichroism (ECD) analysis supported the *R*-configuration of C4-hydroxy in **10** with a positive cotton effect at 228 nm (Figure S17). In addition to a small amount of the aldehyde product **8** (1.8%), $OleT_{JE}$ was also able to

further oxidize **10** into 4-keto-*cis*-2-dodecenoic acid (**11**; 8.9%) only in the AldO/glycerol-based H_2O_2 releasing system (Table S3, Figures S18–S26). In comparison, the substrate conversion ratio of **3** (43.2%) was significantly lower than that of **2** (100%). To our surprise, 6*S*-hydroxy-*trans*-2-dodecenoic acid (**12**; 75.8%, Figure 1g) turned out to be the main product of the *trans*-α,β-unsaturated fatty acid **3**, demonstrating an unprecedented regio- and stereoselectivity. The structure and stereochemistry of the C6-hydroxy of **12** was determined using the Mosher ester method (Table S4, Figures S27–S40). $OleT_{JE}$ also stereoselectively hydroxylated the C–H bond at C5, giving rise to the minor product 5*R*-hydroxy-*trans*-2-dodecenoic acid (**13**; 22.7%; see Table S5 and Figures S41–S51 for structural determination). The substantial difference in specific rotations of **12** ($[\alpha]_D^{20} = 3.21$) and **13** ($[\alpha]_D^{20} = -5.03$) further supports their opposite configurations. Notably, no alkyne product (1-undecyne) was detected in all reactions (Figure S52), indicating that no typical decarboxylation occurred. Instead, a trace amount of **8** was observed. Collectively, **2** and **3**, as a pair of *cis–trans*-isomers, gave distinct conversion efficiencies and product profiles in the $OleT_{JE}$-catalyzed reactions (Figures 1d,g).

To rationalize the distinct regioselectivity of $OleT_{JE}$ towards **2** and **3**, we performed molecular docking using Sybyl-X 2.0 software.[9] As shown in Figure 2a, the docking conformation of the *cis*-isomer **2** in the active site of $OleT_{JE}$ is analogous to the *cis*-like configuration seen both in the co-crystal structure of $OleT_{JE}$ and the C_{20} substrate arachidic acid (PDB ID code: 4L40)[10] and the docking structure of **1** in $OleT_{JE}$ (Figure S53). These results suggest that the C2–C3 *cis*-configuration might be favored by the architecture of $OleT_{JE}$ active site. In this binding mode, the shorter distance between the *pro*-4*R* C–H bond (relative to the *pro*-4*S* C–H bond) and the heme-iron may also explain the stereoselectivity of $OleT_{JE}$ towards **2** (Figure 2a). Interestingly, the *trans*-isomer **3** binds to $OleT_{JE}$ in a "U-shape" with the turning points at C5 and C6 (Figure 2b), which is similar to the reported $P450_{Biol}$-mediated hydroxylation of the central carbons of a fatty acyl chain.[11] In this binding mode, the *pro*-5*R* and *pro*-6*S* C–H bonds to be differentially hydroxylated are 4.1 Å and 5.0 Å (versus 5.3 Å and 5.8 Å for the *pro*-5*S* and *pro*-6*R* C–H bonds, respectively) away from the heme-iron reactive center, qualitatively explaining the regio- and stereoselectivity (5*R*- and 6*S*-hydroxylation) of $OleT_{JE}$ towards **3**.

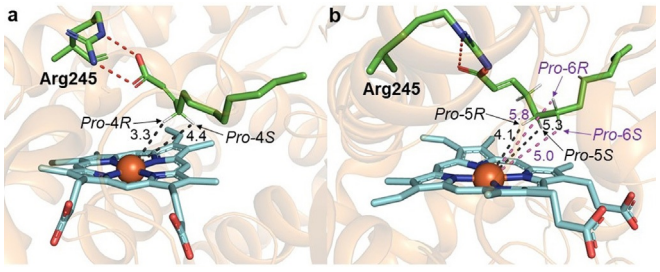

Figure 2. Docking structures of a) *cis*-2-dodecenoic acid (**2**) and b) *trans*-2-dodecenoic acid (**3**) in the active site of $OleT_{JE}$ (PDB ID code: 4L40). In the top 20 lowest energy docking solutions, (a) and (b) are found to adopt the ideal catalytic conformations. The distances in Ångstrom [Å] are indicated by the dashed lines.

Identification of the unexpected C–C bond cleavage products of fatty acid hydroxylase $P450_{BSβ}$ and $P450_{SPα}$. Motivated by the unexpected reactivity of $OleT_{JE}$ against the α,β-unsaturated fatty acids, we further investigated the activities of $P450_{SPα}$ and $P450_{BSβ}$ towards **1**–**3**. Consistent with the previous report,[4d] $P450_{SPα}$ almost exclusively catalyzed the α-hydroxylation of **1** at a conversion of 100%, leading to the predominant product **5** (94.6%). Unexpectedly, we also observed two previously unreported aldehyde products **8** (2.5%) and decanal (**9**; 2.9%) in trace amounts (Figure 1c). By contrast, $P450_{BSβ}$ completely transformed **1** into a mixture of **4** (12.5%), **5** (38.6%), **6** (33.9%), **7** (10.5%), and **8** (4.5%) (Figure 1b).

Unlike $OleT_{JE}$, both $P450_{SPα}$ and $P450_{BSβ}$ demonstrated similar catalytic behaviors towards the *cis–trans*-isomers **2** and **3**, leading to the common main product of **8** and the side products of **7** and **9** (Figure 1e,f,h,i, Figures S54–S61). Moreover, the epoxide products 2*R*,3*R*-epoxy-dodecanoic acid (**14**, $[\alpha]_D^{20} = -9.09$) and 2*S*,3*S*-epoxy-dodecanoic acid (**15**) with opposite stereochemistry were generated from **2** by $P450_{BSβ}$ and $P450_{SPα}$, respectively (Figure 1e,f, Table S6, Figures S62–S76). Interestingly, a favored formation of 2*R*,3*S*-epoxy-dodecanoic acid (**16**, $[\alpha]_D^{20} = -6.56$) by $P450_{BSβ}$ and $P450_{SPα}$ was observed consistently for the *trans*-isomer **3**. (Figure 1h,i, Table S7, Figures S77–S86).

Of note, $P450_{BSβ}$, but not $P450_{SPα}$, was also capable of hydroxylating **2** and **3** to **10** and **12** (also seen in the $OleT_{JE}$-mediated reactions, Figure 1d,g), respectively (Figure 1, Figures S54 and S59), likely due to the differences in their substrate binding pockets. Specifically, the active site cavity of $P450_{SPα}$ is smaller than that of $P450_{BSβ}$ (similar to $OleT_{JE}$), and their hydrophobic channels adopt different orientations,[4c,d] thus leading the substrates (**1**, **2**, and **3**) to be more perpendicular to the heme plane of $P450_{SPα}$ (Figures S87,S88). Again, no alkyne product (1-undecyne) was observed in the reactions catalyzed by either $P450_{BSβ}$ or $P450_{SPα}$ (Figure S89).

Mechanistic analysis for undecanal formation. To explain the intriguing mechanisms for the efficient carbon–carbon bond cleavage of *cis*-2-dodecenoic acid (**2**) by $P450_{SPα}$ leading to the unexpected products **7**–**9** (especially the main product **8**, Figure 1f), we first confirmed that **7**–**9** and 2*S*,3*S*-epoxy-dodecanoic acid (**15**) were all stable end products (Figures S90–S93). Next, using the ^{18}O-labeled $H_2{}^{18}O_2$, we determined that the oxygen atom in **7**–**9** and **15** is unanimously derived from hydrogen peroxide since the ^{18}O-incorporation was observed by GC–MS analysis (Figures S94–S97).

For the production of the aldehyde **8** from either **2** or **3** by $P450_{SPα}$ and $P450_{BSβ}$, we initially hypothesized that the reactions might involve the sequential $C_α$-hydroxylation, isomerization to α-keto fatty acid, and oxidative decarboxylation (analogous to the reported α-keto acid decarboxylase).[12] To test this hypothesis, the tentative transformation of α-keto-dodecanoic acid (**17**) into **8** by $P450_{SPα}$ or $P450_{BSβ}$ was conducted. Briefly, **17** was prepared from **1** by an enzymatic cascade in one pot: **1** was first α-hydroxylated by $P450_{SPα}$ to **5**, which was in turn oxidized to **17** by the (*S*)-α-hydroxyacid oxidase from *Aerococcus viridans*[13] with internal H_2O_2 recycling (Figure S98). However, no further $P450_{SPα}$-mediated decarboxylation of **17** to **8** was observed (Figur-

es S99,S100), indicating that the α-keto fatty acid is not a precursor of **8**.

To unravel the mechanism of $P450_{SPα}$-catalyzed aldehyde (**8**) formation from **2**, combined molecular dynamics (MD) simulations and quantum mechanics/molecular mechanics (QM/MM) calculations were conducted. In the initial reactant complex of Fe^{III}–H_2O_2 (**RC**, Figure 3), H_2O_2 forms a strong H-bond with the carboxylate group of fatty acid, suggesting that the fatty acid substrate plays a key role in stabilizing H_2O_2. Starting from **RC**, we investigated two competing reaction pathways. In one pathway that transpires via the heterolytic O–O cleavage (Figure 3), the proton transferred from proximal hydroxy (-O1H1) of H_2O_2 to the O3 atom of the substrate, which is coupled with the H-bond shift from O1 to O2, thereby generating the ferric hydroperoxide species (Cpd 0, i.e., **IC1**). The subsequent O–O heterolysis in Cpd 0, which is triggered by the proton transfer from O3 to O2, affords the active species of Cpd I (i.e., **IC2**).[14] As shown in Figure 3, the Cpd I formation requires overcoming an energy barrier of 15.2 kcal mol^{-1} (**RC**→**TS2**). In the alternative but unfavorable mechanistic route, the formation of Cpd I is initiated by the homolytic O–O cleavage mechanism,[15] which involves an energy barrier of 21.6 kcal mol^{-1} (Figure S101). Obviously, the heterolysis mechanism (Figure 3) is much favored over the homolysis mechanism (Figure S101) in Cpd I generation.

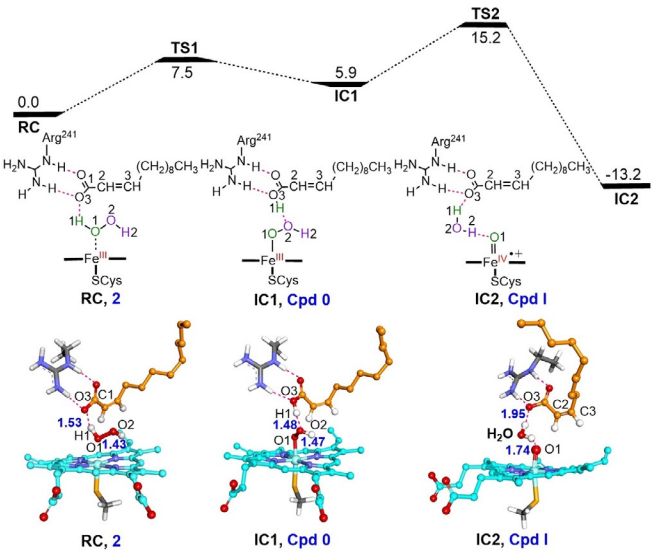

Figure 3. The calculated mechanism (with energies in kcal mol^{-1}) for the formation of Cpd I by $P450_{SPα}$ in the presence of the substrate *cis*-2-dodecenoic acid (**2**). The fatty acid carboxylate group interacting with the guanidyl group of Arg^{241} is located above the heme. The key distances are given in Ångstrom [Å].

Starting from the Cpd I/**2** complex **IC2′**, we investigated two competing pathways (Figure 4). The one on the right (in blue profile) involves oxygen atom transfer from Cpd I to C2 of the double bond in substrate, which involves a small barrier of 16.6 kcal mol^{-1} (**IC2′**→**TS3**), leading to the C3-centered substrate radical intermediate **IC3**. Further C3–O1 coupling is quite facile, which only overcomes a slight barrier of 1.9 kcal mol^{-1} (**IC3**→**TS4**), leading to the formation of epoxidation product, 2*S*,3*S*-epoxy-dodecanoic acid (**PC**, **15**). In the other pathway on the left (the red profile), the reaction is initiated by the H-abstraction from H2 of the adjacent water molecule derived from H_2O_2 activation (**IC2′**→**TS3′**), which is coupled with the attack of water O2 onto the C2 site

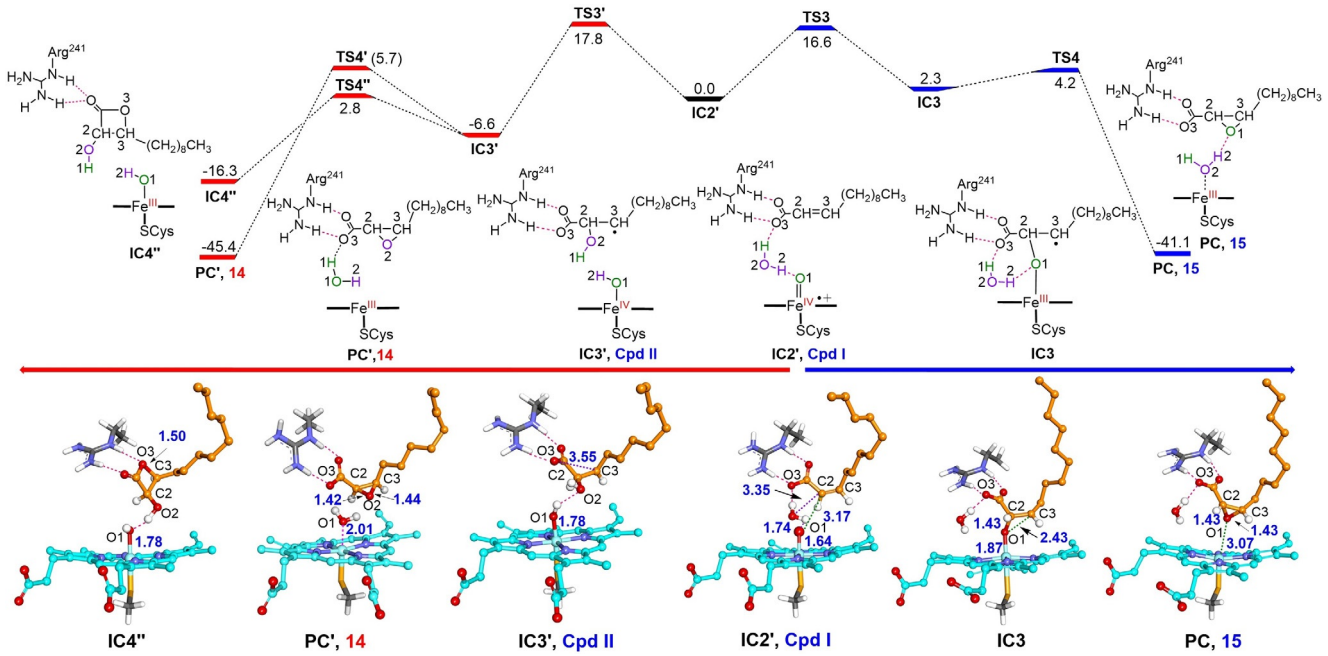

Figure 4. QM/MM-calculated mechanisms (with energies in kcal mol^{-1}) for the formation of four-membered ring lactone intermediate (**IC4″**) and 2*S*,3*S*-epoxy-dodecanoic acid (**PC**, **15**) from *cis*-2-dodecenoic acid (**2**) starting from Cpd I of $P450_{SPα}$, along with the QM/MM-optimized structures of key species involved in the reactions. The fatty acid carboxylate group interacting with the guanidyl group of Arg^{241} is located above the heme. The key distances are given in Ångstrom [Å].

of substrate. The water molecule, derived from H_2O_2 activation, is stable during the long-time MD simulation (Figure S102). And this reaction pathway experiences a barrier of 17.8 kcal mol^{-1} (**IC2′→TS3′**), giving rise to the formation of Fe^{IV}–OH species (Cpd II) and the C2-hydroxylated substrate radical intermediate **IC3′**. Stemming from **IC3′**, we considered two competing pathways. The one via **TS4′** involves the H1 abstraction from O2 by Cpd II, which is coupled with the O2–C3 bond formation. This reaction requires overcoming a barrier of 12.3 kcal mol^{-1} (**IC3′→TS4′**), thus forming the epoxide product 2*R*,3*R*-epoxy-dodecanoic acid (**PC′, 14**). In the alternative pathway via **TS4″**, the nucleophilic attack of the substrate O3 onto the substrate C3 is coupled with the electron transfer from the substrate to Cpd II, which involves a barrier of 9.4 kcal mol^{-1} and affords the four-membered ring intermediate **IC4″**. Obviously, the formation of the four-membered ring intermediate is kinetically favored over the epoxide formation pathway (**IC3′→TS4′**). Thus, the reaction on the left (the red profile) would lead to the main intermediate of four-membered ring **IC4″**.

We further investigated the transformation of 2-epoxide (**14** and **15**) and four-membered ring intermediate in water solution with hybrid cluster-continuum (HCC) model calculations (see Figures S103–S105 for details).[16] Our calculations (Figure S103) showed that the acid-catalyzed ring opening of 2-epoxide needs to overcome a very high energy barrier of 25.2 kcal mol^{-1}, thus being infeasible in water solution, which is consistent with our experimental result (Figure S93). Therefore, we propose a new mechanism for aldehyde formation from the four-membered ring intermediate (Figure 5). Briefly, the transformation of **IC4″** could be mediated by the acid–base catalysis of the carboxylic group from either the substrate itself or the surface residues of enzyme (such as Asp or Glu) in the reaction system. Indeed, our calculations showed that the nucleophilic attack of carboxylate onto C3 of **IC4″**, which is coupled with the C3–O3 cleavage, generates the 3-acyloxylated intermediate **IC5**. The following C1–C2 bond cleavage in **IC5** is coupled with the dissociation of the carboxylate group, leading to the formation of enol **IC6** and CO_2. The final enol–keto isomerization would afford the final product of aldehyde **PC″** (i.e., **8**; see Figures S104,S105 for details). Thus, our calculations support that the oxygen atoms in both **8** and epoxide **15** should originate from H_2O_2, which is consistent with the isotopically labeled $H_2{}^{18}O_2$ tracing experiments (Figures S95 and S97) as described above.

In addition, we attempted to explain the generation of minor products **9** and **7** (Figures S106–S111). The formation of **7** is similar to that of **8** with the departure of one molecular

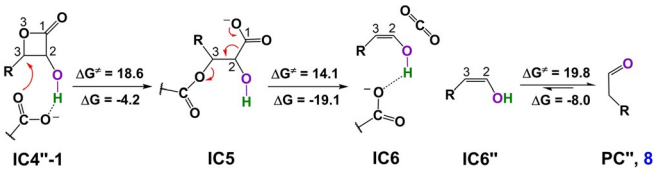

Figure 5. The proposed reaction mechanism (with energies in kcal mol^{-1}) from the four-membered ring lactone intermediate (**IC4″-1**) to aldehyde (**8**) in aqueous solution.

of CO_2; the difference is that the water OH derived from H_2O_2 activation attacks the substrate's C3 site (other than C2 for **8**) to afford the three-membered ring intermediate. A mechanism involving diol cleavage by Cpd I was proposed for the C_{10} aldehyde product **9**, which is similar to the C–C bond cleavage route of $P450_{SCC}$ and $P450_{BioI}$.[17] To consolidate this mechanism, glyoxylic acid, the predicted C–C bond cleaved product, was successfully detected by LC–MS analysis of the 2,4-dinitrophenylhydrazine-derivatized sample (Figures S112–S120).[18]

Reactivity of CYP152 peroxygenases. It is interesting that the overall substrate conversions of these CYP152 peroxygenases largely varied (Table 1). Of note, the catalytic activities supported by the AldO/glycerol-based in situ H_2O_2 releasing system were unanimously higher than those of the exogenous H_2O_2 addition system. In the case of $OleT_{JE}$, the highest turnover number (TON) was achieved by substrate **2** (TON = 990, conversion = 99%, Table 1), which is 21.5 times higher than that of substrate **3** (TON = 44, 4.4%). Consistently, the dissociation constant (K_D) values determined by substrate titration experiments[19] revealed tighter binding of **2** than both **1** and **3** (1.7 ± 0.1 μM versus 3.2 ± 0.2 μM and 4.1 ± 0.4 μM, respectively; Table S8, Figure S121). Similarly, the preference of the *cis*-isomer **2** over the *trans*-isomer **3** was shown as a common phenomenon for $P450_{SP\alpha}$ and $P450_{BS\beta}$ (Table 1). It is worth noting that $P450_{SP\alpha}$ showed the highest TON of 14381 towards **2** when supported by the in situ H_2O_2-generating system at 30 °C for 24 h (Table S9). Moreover, the K_D values of **2** were similar to those of **1** for $P450_{BS\beta}$ (1.9 ± 0.2 μM versus 1.8 ± 0.2 μM) and $P450_{SP\alpha}$ (1.9 ± 0.4 μM versus 1.8 ± 0.3 μM; Table S8, Figures S122,S123), which is consistent with the corresponding catalytic activities (Table 1). Besides, $P450_{SP\alpha}$ and $P450_{BS\beta}$ could still maintain high catalytic activity in the presence of H_2O_2 up to 10 mM with the highest conversion of 23.1% (TON = 2307), demonstrating superior H_2O_2 tolerance far beyond $OleT_{JE}$ (Table 1, Table S9), which is consistent with the previous studies.[20] As in situ H_2O_2-generating system further increased the TON of $P450_{SP\alpha}$ to 9207 under the same reaction conditions, we reason that a CYP152 peroxygenase supported by the in situ H_2O_2-generating system is a more productive and sustainable enzymatic system for future practical applications.

Conclusion

In summary, this study provides the first insights into the reactivity of CYP152 peroxygenases towards α,β-unsaturated fatty acids. The presence of the C_α=C_β double bond dramatically changes the chemo- and regioselectivity of $OleT_{JE}$, $P450_{SP\alpha}$, and $P450_{BS\beta}$, likely due to the shortened bond length, the different electronic property, and the conformation-fixing effect of the double bond, which would lead to the changed substrate positioning (relative to the saturated fatty acid with the same carbon chain length) in the subtly different active sites of the three P450 enzymes. The preference of the C2–C3 *cis*-configuration over the *trans*-configuration is a common phenomenon for the three studied CYP152 family members due to the *cis*-favoring topology of their substrate binding

Table 1: The conversions of substrates **1**–**3** to different products by the three representative CYP152 peroxygenases in the two different H_2O_2-supplying systems.

Enzyme	Substrate	mM	TON[a]	TON[b]	Conversion [%]	Products
$OleT_{JE}$	**1**	0.5	440 ± 3	500	88.1[a]/100[b]	**4**–**8**
		1	102 ± 10	189 ± 30	10.2[a]/18.9[b]	**4**
		2	0	113 ± 39	0[a]/5.7[b]	**4**
	2	0.5	465 ± 17	500	93.1[a]/100[b]	**10**, **11***, **8**
		1	704 ± 44	990 ± 3	70.4[a]/99[b]	**10**, **11***, **8**
		2	0	71 ± 31	0[a]/3.6[b]	**10**
	3	0.5	75 ± 7	215 ± 26	15.2[a]/43.2[b]	**12**, **13**, **8**
		1	0	44 ± 8	0[a]/4.4[b]	**12**
$P450_{SP\alpha}$	**1**	0.5	317 ± 36	500	63.4[a]/100[b]	**5**, **8**, **9**
		1	534 ± 25	1000	53.4[a]/100[b]	**5**, **8**, **9**
		5	3336 ± 273	4877 ± 22	66.7[a]/97.5[b]	**5**, **8**, **9**
		10	2307 ± 247	9207 ± 247	23.1[a]/92.1[b]	**5**, **8**, **9**
	2	0.5	283 ± 3	500	56.6[a]/100[b]	**7**–**9**, **15**
		1	416 ± 21	1000	41.6[a]/100[b]	**7**–**9**, **15**
		5	547 ± 213	4826 ± 8	10.9[a]/96.5[b]	**7**–**9**, **15**
		10	1714 ± 122	6708 ± 25	17.1[a]/67.1[b]	**7**–**9**, **15**
	3	0.5	14 ± 7	58 ± 9	2.8[a]/11.6[b]	**7**–**9**, **16**
		1	27 ± 12	86 ± 7	2.7[a]/8.6[b]	**7**–**9**, **16**
$P450_{BS\beta}$	**1**	0.5	320 ± 4	500	64.1[a]/100[b]	**4**–**8**
		1	201 ± 21	989 ± 1	20.1[a]/98.9[b]	**4**–**8**
		5	340 ± 84	4404 ± 142	6.8[a]/88.1[b]	**4**–**8**
		10	816 ± 11	5181 ± 281	8.2[a]/51.8[b]	**4**–**8**
	2	0.5	131 ± 2	500	26.2[a]/100[b]	**7**–**10**, **14**
		1	227 ± 2	996	22.7[a]/99.6[b]	**7**–**10**, **14**
		5	763 ± 241	3767 ± 77	15.3[a]/75.3[b]	**7**–**10**, **14**
		10	557 ± 105	1177 ± 319	5.6[a]/11.8[b]	**7**–**10**, **14**
	3	0.5	0	289 ± 13	0[a]/57.8[b]	**7**–**9**, **12**, **16**
		1	0	534 ± 26	0[a]/53.4[b]	**7**–**9**, **12**, **16**
		2	0	187 ± 11	0[a]/9.4[b]	**7**–**9**, **16**

[a] Reaction conditions: 1 μM P450 supported by exogenous H_2O_2 with the same molar amount as the substrate at 30 °C for 6 h. [b] Reaction conditions: 1 μM P450 supported by the 5 μM AldO + 10% glycerol system, at 30 °C for 6 h. * A small amount of product **11** appeared only in the AldO/glycerol-based in situ H_2O_2 generating system.

pockets. The binding of the unfavorable *trans*-isomer may require torsion of the fatty acyl chain to some extent, thus leading to a larger entropy penalty of substrate binding.

The combined isotopically labeled $H_2{}^{18}O_2$ tracing experiments, MD simulations, and QM/MM calculations unravel a highly uncommon mechanism for the Cpd I-mediated aldehyde formation, which is initiated by the H-abstraction from the adjacent water rather than commonly from the C–H bond of the substrate. This unusual event is coupled with the attack of water OH that is derived from H_2O_2 activation onto the substrate C2 site, leading to the formation of Cpd II and the key C2-hydroxylated substrate radical. Then, Cpd II accepts a single electron transfer from the substrate and triggers the formation of a four-membered ring intermediate, which further loses CO_2 by acid–base catalysis in water solution and rearranges to form undecanal. This finding expands our understanding of the mechanism of CYP152 peroxygenases for the C–C bond cleavage reactions. This mechanism is totally different from the C–C scission reaction of the saturated fatty acid by $OleT_{JE}$, which is initiated by a typical substrate C_β–H abstraction, and followed by a similar single electron transfer to the heme, thus leading to a carbocation poise for later C–C bond cleavage to liberate CO_2.[5a,b]

The present study not only proposes the key role of the active site water derived from H_2O_2 activation in the catalysis of CYP152 peroxygenases for the first time, but also provides a new, simple, and more productive enzymatic system for aldehyde biosynthesis compared with the reported biocatalytic aldehyde-producing systems.[21] An important question to be answered is whether the aldehyde-forming mechanism is also applicable for other α,β-unsaturated fatty acids with different chain length. To our delight, both $P450_{SP\alpha}$ and $P450_{BS\beta}$ indeed produced the aldehyde products lauraldehyde (C_{12}) and tridecanal (C_{13}) as the main products from *trans*-2-tridecenoic acid (C_{13}) and *trans*-2-tetradecenoic acid (C_{14}), respectively (Figures S124,S125). However, due to the commercial unavailability, we were unable to test more substrates,

especially the *cis*-isomers. Thus, further studies using synthesized substrates are required for a more general conclusion.

Of note, a high TON of 14381 was achieved for $P450_{SP\alpha}$ towards **2** with the in situ H_2O_2-generating system, showing great potential as an applicable biocatalyst to synthesize fatty aldehydes and other downstream products. Fatty aldehydes (C_8–C_{13}) have long served as flavor and fragrance components; they also represent the essential metabolic intermediates for microbial synthesis of various industrially relevant oleochemicals.[22] Furthermore, the unexpected products C6-hydroxy-2-dodecenoic acid (**12**) and C5-hydroxy-2-dodecenoic acid (**13**) of $OleT_{JE}$ towards the *trans*-isomer **3** can be saponified to obtain the analogues of Massoia lactone,[23] which have anti-fungal, anti-cancer and anti-viral activities, thus holding significant application potential in the pharmaceutical and biomedical sectors.

Acknowledgements

This work was supported by the National Key Research and Development Program of China (2019YFA0905100 and 2019YFA0706900), National Natural Science Foundation of China (32025001 to S.L. and 22073077 to B.W.), the Natural Science Foundation of Shandong Province, China (ZR2019ZD20), the Laboratory for Marine Drugs and Bioproducts of Pilot National Laboratory for Marine Science and Technology (Qingdao) (LMDBKF-2019-01), and the Tianjin Synthetic Biotechnology Innovation Capability Improvement Project (TSBICIP-KJGG-001). We thank Ms. Cong Wang at Qingdao Institute of Bioenergy and Bioprocess Technology, Chinese Academy of Sciences and Dr. Jingyao Qu (Shandong University) for their assistance in GC–MS and LC–HRMS data collection.

Conflict of Interest

The authors declare no conflict of interest.

Keywords: CYP152 peroxygenases · molecular dynamics simulations · QM/MM calculations · substrate probes · α,β-unsaturated fatty acids

[1] a) M. J. Coon, *Annu. Rev. Pharmacol. Toxicol.* **2005**, *45*, 1–25; b) Z. Li, Y. Jiang, F. P. Guengerich, L. Ma, S. Li, W. Zhang, *J. Biol. Chem.* **2020**, *295*, 833–849.

[2] a) A. W. Munro, K. J. McLean, J. L. Grant, T. M. Makris, *Biochem. Soc. Trans.* **2018**, *46*, 183–196; b) X. Zhang, S. Li, *Nat. Prod. Rep.* **2017**, *34*, 1061–1089.

[3] a) M. A. Rude, T. S. Baron, S. Brubaker, M. Alibhai, S. B. Del Cardayre, A. Schirmer, *Appl. Environ. Microbiol.* **2011**, *77*, 1718–1727; b) J. Belcher, K. J. McLean, S. Matthews, L. S. Woodward, K. Fisher, S. E. J. Rigby, D. R. Nelson, D. Potts, M. T. Baynham, D. A. Parker, D. Leys, A. W. Munro, *J. Biol. Chem.* **2014**, *289*, 6535–6550.

[4] a) I. Matsunaga, A. Ueda, N. Fujiwara, T. Sumimoto, K. Ichihara, *Lipids* **1999**, *34*, 841–846; b) I. Matsunaga, T. Sumimoto, A. Ueda, E. Kusunose, K. Ichihara, *Lipids* **2000**, *35*, 365–371; c) D. S. Lee, A. Yamada, H. Sugimoto, I. Matsunaga, H. Ogura, K. Ichihara, S. Adachi, S. Y. Park, Y. Shiro, *J. Biol. Chem.* **2003**, *278*, 9761–9767; d) T. Fujishiro, O. Shoji, S. Nagano, H. Sugimoto, Y. Shiro, Y. Watanabe, *J. Biol. Chem.* **2011**, *286*, 29941–29950; e) L. Hammerer, M. Friess, J. Cerne, M. Fuchs, G. Steinkellner, K. Gruber, K. Vanhessche, T. Plocek, C. K. Winkler, W. Kroutil, *ChemCatChem* **2019**, *11*, 5642–5649; f) H. Chen, M. Huang, W. Yan, W. Bai, X. Wang, *ACS Catal.* **2021**, *11*, 10625–10630.

[5] a) J. L. Grant, C. H. Hsieh, T. M. Makris, *J. Am. Chem. Soc.* **2015**, *137*, 4940–4943; b) J. L. Grant, M. E. Mitchell, T. M. Makris, *Proc. Natl. Acad. Sci. USA* **2016**, *113*, 10049–10054; c) A. S. Faponle, M. G. Quesne, S. P. de Visser, *Chem. Eur. J.* **2016**, *22*, 5478–5483; d) C. H. Hsieh, X. Huang, J. A. Amaya, C. D. Rutland, C. L. Keys, J. T. Groves, R. N. Austin, T. M. Makris, *Biochemistry* **2017**, *56*, 3347–3357.

[6] a) S. Matthews, J. D. Belcher, K. L. Tee, H. M. Girvan, K. J. McLean, S. E. Rigby, C. W. Levy, D. Leys, D. A. Parker, R. T. Blankley, A. W. Munro, *J. Biol. Chem.* **2017**, *292*, 5128–5143; b) B. Fang, H. Xu, Y. Liu, F. Qi, W. Zhang, H. Chen, C. Wang, Y. Wang, W. Yang, S. Li, *Sci. Rep.* **2017**, *7*, 44258; c) J. A. Amaya, C. D. Rutland, N. Leschinsky, T. M. Makris, *Biochemistry* **2018**, *57*, 344–353; d) J. B. Wang, R. Lonsdale, M. T. Reetz, *Chem. Commun.* **2016**, *52*, 8131–8133; e) C. H. Hsieh, T. M. Makris, *Biochem. Biophys. Res. Commun.* **2016**, *476*, 462–466; f) H. Xu, L. Ning, W. Yang, B. Fang, C. Wang, Y. Wang, J. Xu, S. Collin, F. Laeuffer, L. Fourage, S. Li, *Biotechnol. Biofuels* **2017**, *10*, 208; g) Y. Liu, C. Wang, J. Yan, W. Zhang, W. Guan, X. Lu, S. Li, *Biotechnol. Biofuels* **2014**, *7*, 28; h) Y. Jiang, Z. Li, C. Wang, Y. J. Zhou, H. Xu, S. Li, *Biotechnol. Biofuels* **2019**, *12*, 79.

[7] a) M. Pickl, S. Kurakin, F. G. Cantu Reinhard, P. Schmid, A. Pocheim, C. K. Winkler, W. Kroutil, S. P. de Visser, K. Faber, *ACS Catal.* **2019**, *9*, 565–577; b) F. G. C. Reinhard, Y. T. Lin, A. Stanczak, S. P. de Visser, *Molecules* **2020**, *25*, 2675; c) A. S. Chowdhury, H. S. Ali, A. S. Faponle, S. P. de Visser, *Phys. Chem. Chem. Phys.* **2020**, *22*, 27178–27190.

[8] a) S. Matthews, K. L. Tee, N. J. Rattray, K. J. McLean, D. Leys, D. A. Parker, R. T. Blankley, A. W. Munro, *FEBS Lett.* **2017**, *591*, 737–750; b) Y. Jiang, Z. Li, S. Zheng, H. Xu, Y. J. Zhou, Z. Gao, C. Meng, S. Li, *Biotechnol. Biofuels* **2020**, *13*, 52.

[9] Y. Zhao, C. Zhao, J. Lu, J. Wu, C. Li, Z. Hu, W. Tian, L. Yang, J. Xiang, H. Zhou, Z. Deng, J. Huang, K. Hong, *Pharmacol. Res.* **2019**, *146*, 104294.

[10] J. Belcher, K. J. McLean, S. Matthews, L. S. Woodward, K. Fisher, S. E. Rigby, D. R. Nelson, D. Potts, M. T. Baynham, D. A. Parker, D. Leys, A. W. Munro, *J. Biol. Chem.* **2014**, *289*, 6535–6550.

[11] M. J. Cryle, I. Schlichting, *Proc. Natl. Acad. Sci. USA* **2008**, *105*, 15696–15701.

[12] a) M. Wang, L. Zhang, K. H. Boo, E. Park, G. Drakakaki, F. Zakharov, *Plant. J.* **2019**, *98*, 112–125; b) S. Gandomkar, A. Dennig, A. Dordic, L. Hammerer, M. Pickl, T. Haas, M. Hall, K. Faber, *Angew. Chem. Int. Ed.* **2018**, *57*, 427–430; *Angew. Chem.* **2018**, *130*, 434–438.

[13] K. Yorita, K. Aki, T. Ohkuma-Soyejima, T. Kokubo, H. Misaki, V. Massey, *J. Biol. Chem.* **1996**, *271*, 28300–28305.

[14] a) S. Shaik, S. Cohen, Y. Wang, H. Chen, D. Kumar, W. Thiel, *Chem. Rev.* **2010**, *110*, 949–1017; b) J. B. Wang, Q. Huang, W. Peng, P. Wu, D. Yu, B. Chen, B. Wang, M. T. Reetz, *J. Am. Chem. Soc.* **2020**, *142*, 2068–2073; c) J. Rittle, M. T. Green, *Science* **2010**, *330*, 933–937.

[15] B. Wang, C. Li, K. D. Dubey, S. Shaik, *J. Am. Chem. Soc.* **2015**, *137*, 7379–7390.

[16] a) B. Wang, Z. Cao, *J. Phys. Chem. A* **2010**, *114*, 12918–12927; b) H. Zhou, B. Wang, F. Wang, X. Yu, L. Ma, A. Li, M. T. Reetz, *Angew. Chem. Int. Ed.* **2019**, *58*, 764–768; *Angew. Chem.* **2019**, *131*, 774–778.

[17] a) M. J. Cryle, J. J. De Voss, *Chem. Commun.* **2004**, 86 – 87; b) F. K. Yoshimoto, I. J. Jung, S. Goyal, E. Gonzalez, F. P. Guengerich, *J. Am. Chem. Soc.* **2016**, *138*, 12124 – 12141; c) H. Su, B. Wang, S. Shaik, *J. Am. Chem. Soc.* **2019**, *141*, 20079 – 20088.
[18] a) Y. Mao, X. Wang, S. Tang, H. Yang, Y. Xie, *Anal. Methods* **2015**, *7*, 6207 – 6212; b) M. El-Maghrabey, H. Suzuki, N. Kishikawa, N. Kuroda, *Talanta* **2021**, *233*, 122522.
[19] S. Li, H. Ouellet, D. H. Sherman, L. M. Podust, *J. Biol. Chem.* **2009**, *284*, 5723 – 5730.
[20] a) A. Dennig, M. Kuhn, S. Tassoti, A. Thiessenhusen, S. Gilch, T. Bulter, T. Haas, M. Hall, K. Faber, *Angew. Chem. Int. Ed.* **2015**, *54*, 8819 – 8822; *Angew. Chem.* **2015**, *127*, 8943 – 8946; b) S. Wang, S. Jiang, H. Chen, W. Bai, X. Wang, *ACS Catal.* **2020**, *10*, 14375 – 14379.
[21] V. Kazimírová, M. Rebroš, *Int. J. Mol. Sci.* **2021**, *22*, 4949.
[22] a) T. Lehtinen, E. Efimova, S. Santala, V. Santala, *Microb. Cell Fact.* **2018**, *17*, 19; b) S. Maurer, H. Schewe, J. Schrader, M. Buchhaupt, *J. Biotechnol.* **2019**, *305*, 11 – 17.
[23] a) A. Pons, L. Allamy, V. Lavigne, D. Dubourdieu, P. Darriet, *Food Chem.* **2017**, *232*, 229 – 236; b) J. Manning, M. Tavanti, J. L. Porter, N. Kress, S. P. De Visser, N. J. Turner, S. L. Flitsch, *Angew. Chem. Int. Ed.* **2019**, *58*, 5668 – 5671; *Angew. Chem.* **2019**, *131*, 5724 – 5727.

Manuscript received: August 18, 2021
Revised manuscript received: September 6, 2021
Accepted manuscript online: September 15, 2021
Version of record online: October 12, 2021

